Low-Loss Continuously Tunable Optical True Time Delay Based on Si_3N_4 Ring Resonators

Chao Xiang, *Student Member, IEEE*, Michael L. Davenport, Jacob B. Khurgin, *Senior Member, IEEE*, Paul A. Morton, *Fellow, IEEE*, and John E. Bowers, *Fellow, IEEE*

***Abstract*—We design, fabricate, and characterize ultra-low loss continuously tunable optical true time delay devices based on Si_3N_4 ring resonators in a side-coupled integrated spaced sequence of resonators (SCISSOR) structure. A large tunable delay range up to 3.4 ns is demonstrated using the Balanced SCISSOR delay tuning scheme, for a record loss of only 0.89 dB/ns of delay. By optimizing the coupler design a device delay bandwidth of over 10 GHz is achieved with over 0.5 ns maximum time delay. This ultra-low loss delay line can enable distortion free operation for RF signals used in RF beamforming and other applications. Additionally, this device has the potential to be integrated with active photonic components to be part of a fully integrated photonic integrated circuit in an electronically scanned phased array system; utilizing a silicon photonics platform including heterogeneous integration.**

***Index Terms*—Delay lines, optical losses, optical ring resonators, phased arrays, silicon nitride, silicon photonics.**

I. Introduction

RECENT developments in integrated photonics provide new opportunities in a range of applications including data communications [1], [2], optical interconnects [3], and sensing [4]. The benefits of integration to reduced size, weight, and power consumption (SWaP) also greatly improves the performance of various photonic devices and systems [5]. Among them, microwave photonics devices and systems are attracting increasing attention due to the large intrinsic bandwidth of optical signals. The generation, remoting and processing of microwave signals can be achieved in the optical domain, using a mature toolbox of optical devices, [6], including lasers [7]–[10], isolators [11], [12], modulators [13], [14], waveguides [15], and photodetectors [16], [17]. Compared with electrical devices, photonic devices provide low loss, light weight and electromagnetic immune solutions for microwave applications.

Optical true time delay (TTD) is a key element in microwave photonic applications [18]–[20], specifically, in phased-array antennas. Optical TTD provides the same diffraction angle for the wideband frequency components in RF/microwave signals with a large bandwidth. This avoids the beam squint phenomenon of phase delay devices and enables distortion-free operation of the array [21]. In practical electronically scanned phased-array systems, a tunable TTD is required for RF beamforming at different diffraction angles. Integrated on-chip optical TTDs are preferable due to their compact size, significantly improved stability, and ease of integration with a laser source and other key functional elements [22].

There are various approaches to achieve an on-chip tunable optical TTD. Among them, side-coupled integrated spaced sequence of resonators (SCISSOR) based devices have successfully provided a way to achieve a widely tunable optical delay with wide bandwidth and low distortion, by using the Balanced SCISSOR concept [23], [24]. Compared with cascaded optical switch based delay lines, which will have a minimum tuning step size, the Balanced SCISSOR scheme provides a continuously tunable delay [25]. In addition, as SCISSOR devices utilize optical resonances, they can potentially shrink the size of TTD devices compared to those consisting of waveguides with equivalent optical length. Unlike coupled resonator optical waveguide (CROW) delay lines [26], [27], SCISSOR performance does not deteriorate drastically if one of the resonators includes fabrication imperfections, which is important for the practical application of these devices.

For Balanced SCISSOR TTD devices, a longer tunable time delay can be achieved by increasing the number of rings. However, as delay is always proportional to the total optical loss, this delay loss is an ultimate limiting factor of the TTD device performance. Moreover, since detected RF power increases as the square of optical power, every X dB of optical loss results in 2X dB of RF loss, and therefore loss reduction is paramount in microwave photonics applications.

In this paper, we demonstrate a tunable optical delay device based on SCISSOR structures using ultra-low loss Si_3N_4 waveguides. This device has the potential to be integrated with heterogeneously integrated laser, isolator, modulator, and detector devices. When taking advantage of the separate carrier tuning scheme [28], this time delay device can provide very low loss for a large tunable delay range of a wide bandwidth

Manuscript received October 18, 2017; revised December 13, 2017; accepted December 18, 2017. Date of publication December 21, 2017; date of current version January 15, 2018. This work was supported by the Air Force SBIR under Contract # FA8650-15-C-1863 with Morton Photonics. *(Corresponding author: Chao Xiang.)*

C. Xiang, M. L. Davenport, and J. E. Bowers are with the Department of Electrical and Computer Engineering, University of California, Santa Barbara, CA 93106 USA (e-mail: cxiang@ece.ucsb.edu; davenport000@gmail.com; bowers@ece.ucsb.edu).

J. B. Khurgin is with the Department of Electrical and Computer Engineering, Johns Hopkins University, Baltimore, MD 21218 USA (e-mail: jakek@jhu.edu).

P. A. Morton is with the Morton Photonics, West Friendship, MD 21794 USA (e-mail: pmorton@mortonphotonics.com).

Color versions of one or more of the figures in this paper are available online at http://ieeexplore.ieee.org.

Digital Object Identifier 10.1109/JSTQE.2017.2785962

microwave photonic signal. It holds great potential to be a key part of a photonic integrated circuit (PIC) for use in phased-array systems and other applications.

II. Review of Related Research

Optical signals with frequencies of hundreds of THz provide tremendous bandwidth for carrying microwave signals that modulate the envelope of the optical carrier. The microwave modulation signal forms only a very small percentage of the optical carrier frequency. Since modulation will induce a frequency offset between the carrier wave and the sideband, the photonic device must have a bandwidth larger than the microwave signal of interest.

Photonic devices which use optical resonances, such as microresonators, are compact solutions for many applications. However, this usually comes at the expense of a narrow optical bandwidth. In order to be used for microwave photonics, processing carrier and sidebands simultaneously, this typically supports only low signal frequencies, i.e., a small frequency shift between the sidebands (or single sideband) and the optical carrier. However, higher frequency signals are often preferred in phased array antenna designs due to broader signal bandwidth support, and more directional beams for a specific antenna size.

It can be noted that the frequency band between the carrier wave and signal sideband(s) does not carry any information, and so, it would be beneficial to be able to process the carrier and sideband(s) separately. In [28], the separate carrier tuning scheme was proposed and studied; this approach takes a single sideband signal, provides a TTD for the sideband (with a broad signal), while separately providing tuning of the carrier phase (narrowband signal) so that the overall signal looks as though it passed through a wideband TTD device. This approach significantly improves the performance of optical TTD devices, especially for systems with high modulation frequencies. The improvement is by the ratio of the sideband bandwidth to the sideband frequency, e.g., a 1 GHz signal bandwidth on a 60 GHz sideband would see improvements in the TTD figure of merit by 60x by using the separate carrier tuning scheme. For the same delay x bandwidth product, as this scheme greatly lowers the bandwidth requirements to the sideband signal of interest, it allows for a much greater achievable delay range. This opens up the possibility of using optical microresonators with higher finesse in optical TTD devices.

A compact optical TTD device based on silicon microring resonators with a wide bandwidth (10 GHz) and 135 ps delay was demonstrated in [25]. Eight racetrack rings with 7 μm bend radius was employed together with a 7.5 μm straight section to give ~25 ps peak delay per ring resonator. In the ring operating at resonance the third order dispersion of phase $\beta_3 = \partial^3\Phi/\partial\omega^2$ causes quadratic dispersion of the group delay time $\partial^2 T/\partial\omega^2$. The balanced tuning scheme [24] combines equal numbers of resonators whose resonance frequencies are shifted up or down relative to the optical frequency and this arrangement helps to reduce the third order dispersion and thus flatten the time delay spectrum. In addition to the bandwidth improvement, balanced tuning operation enabled fast thermal switching, since the long term transient was canceled during tuning by keeping the device heating constant [29]. Fast thermal switching speed under 10 μs was achieved, applicable to electronically scanned phased array antennas. However, although fabricated in a standard CMOS process, this SCISSOR device showed a relatively high total loss; 3.2 dB loss for a 94 ps delay, corresponding to 4.5 dB/cm propagation loss. If extending to nanosecond scale delay, as needed to support a full antenna aperture, this will give a total loss over 34 dB. In order to lower the loss, a thinner silicon waveguide with 60 nm thickness was employed in [30], but the loss is still as high as 12.4 dB for 1 ns delay.

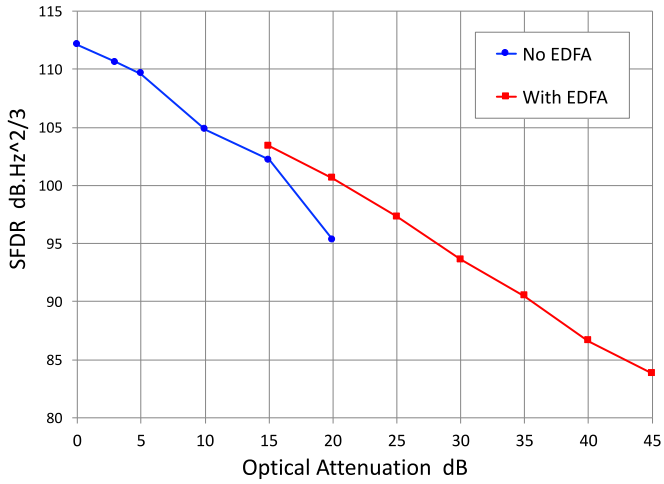

Fig. 1. Measurement of SFDR versus added optical attenuation in an analog optical link, for modulation signals near 10 GHz, showing measurements in a link with and without an EDFA.

The optical loss of TTD devices not only decreases the RF signal power but also has a negative impact on the beamforming system performance, including the key system performance parameter; Spurious Free Dynamic Range (SFDR), as well as link gain and noise figure. This is demonstrated in Fig. 1, which shows the dependence of system SFDR on additional optical loss within a high performance optical analog link - this additional optical loss would be provided by the TTD device when tuning its delay. These measurements were taken using a high power DFB laser followed by a Lithium Niobate optical modulator, followed by a high power, high speed photodetector. For zero (added) attenuation, an SFDR of 112.1 dB.Hz$^{2/3}$ is found for this analog optical link when operated with two microwave tones close to 10 GHz. By adding optical attenuation after the modulator, the SFDR is reduced - along with the received photocurrent. As this attenuation is increased, SFDR falls, initially in a straight line, then the slope of SFDR versus attenuation increases at lower photocurrent due to the increasing effects of thermal noise (higher photocurrent results are shot noise limited).

The curve for SFDR versus attenuation can be extended to larger attenuations by including an Erbium doped fiber amplifier (EDFA) into the link - this provides optical gain to overcome the attenuation, however, this optical gain comes at the cost of additional noise added by the EDFA. The straight line of SFDR versus attenuation using the EDFA follows on from the

no-EDFA curve at higher photocurrent levels (the photocurrent was kept at 10.5 mA when using the EDFA). The clear straight line obtained with and without an EDFA demonstrates a variation in SFDR that is 2/3 of the change in attenuation, i.e., a 6.7 dB drop in SFDR for an increase in attenuation of 10 dB. In high performance analog systems, where SFDR is required to be large, e.g., $>110\,\mathrm{dB.Hz}^{2/3}$ for all delays, then the overall optical attenuation provided by the TTD must remain very small, e.g., <3 dB. This very low TTD attenuation requires extremely low loss optical waveguides and microresonators - as provided by high aspect ratio silicon nitride waveguides [31]. Besides SFDR, the link gain and noise figure will be affected accordingly, degrading the overall system performance.

In order to create lower insertion loss TTD devices, more attention has been paid to reduced propagation loss waveguides such as those using silicon nitride (Si_3N_4). Si_3N_4 provides moderate index contrast with a silicon dioxide (SiO_2) cladding, and when used with very high aspect ratio waveguides [31] are less sensitive to waveguide sidewall roughness. These Si_3N_4 waveguides have much lower propagation loss than silicon waveguides. Additionally, Si_3N_4 waveguides have an ultra-wide transparency band spanning from visible light to mid-IR [32]. Another benefit is their negligible nonlinear absorption loss, which eliminates two photon absorption (TPA) and makes these ultra-low loss waveguides applicable to high power systems. One disadvantage of using Si_3N_4 microresonators compared to using Si microresonators is their larger size, as the minimum bend radius for the lowest loss designs can be far larger than Si devices, e.g., 10x to 100x radius, and so the available space and allowable loss for a specific application will inform the choice of waveguide material and design.

TTD devices based on low loss Si_3N_4 waveguides from the LioniX BV foundry were demonstrated in [33]–[35]. These waveguides use a dual Si_3N_4 stripe geometry for the waveguide, to increase the mode confinement, providing low loss at a reasonably small ring radius of $\sim$100 μm, and offering $\sim$0.1 dB/cm propagation loss. When the loss is decreased, as in this case, it is possible to use a large number of rings. However, due to non-uniformity seen in ring fabrication, each of these rings will have a slightly different resonance frequency, which requires an individual driver and individual tuning. Variations in ring coupling coefficient can give rise to slightly different bandwidths for the different rings, however, the Balanced SCISSOR tunable TTD scheme is quite tolerant to such variations.

Devices including 40 Si_3N_4 ring resonators were developed for use in a high performance phased array antenna application, and were hermetically packaged for use in system level testing [36]. These packaged devices achieved a record tunable delay of 535 ps for a 20 GHz wide signal, 632 ps for a 10 GHz wide signal, with a tunable loss of only 3 dB. A schematic and photo of one of these 40 ring resonator devices is shown in Fig. 2, with a photo of the packaged device (without lid) shown in Fig. 3.

As the number of rings is increased, the driving scheme to individually tune the resonance frequency of each ring becomes more difficult. A concept was proposed to take advantage of the ring resonance non-uniformity [37], while only requiring two driving voltages for all the rings in the Balanced SCISSOR

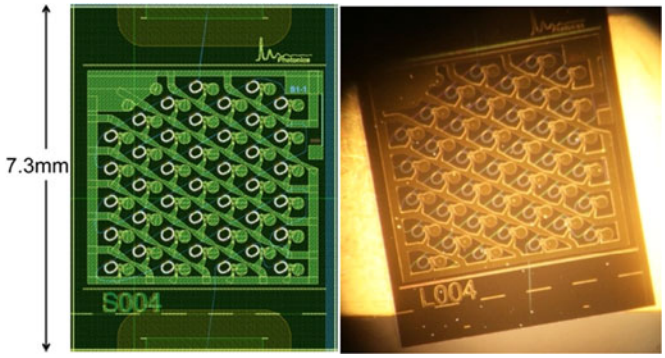

Fig. 2. Layout and photograph of a 40 microresonator TTD device.

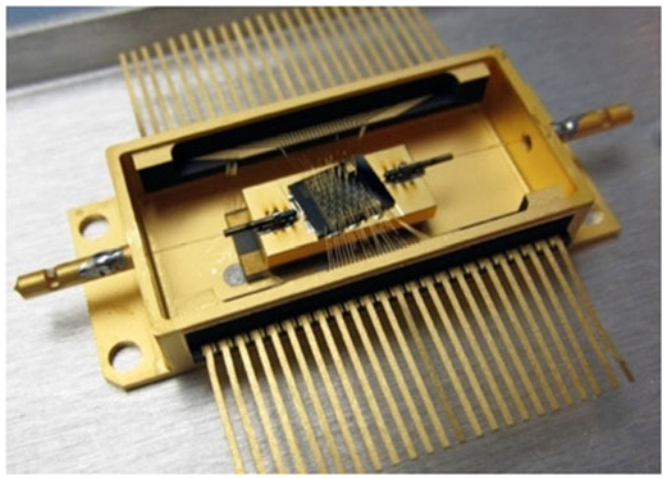

Fig. 3. Photograph showing the inside of a packaged TTD device.

device; this is called the 'Super-Ring' concept. In this approach, half of the rings are tuned together upwards in frequency, and half downwards in frequency, using Balanced SCISSOR tuning. With sufficient number of rings, the overall response of a set of rings looks like that from a single 'Super-Ring,' with broader bandwidth due to resonance frequency variations, and a larger delay from adding all the (linear) delay responses together. Results using 'Super-Ring' tuning were described by Morton [38], additionally, the paper demonstrated high linearity operation, i.e., high SFDR, of an optical link including the packaged TTD device, showing Super-Ring operation providing high SFDR tunable delay of 515 ps for a 20 GHz signal bandwidth, with just two drive voltages. SFDR of over 110 $\mathrm{dB.Hz}^{2/3}$ was maintained for delays up to 300 ps. An example of the tunable time delay from this device is shown in Fig. 4, which shows how a broadband optical pulse is delayed from 0ps to 515 ps using the Balanced SCISSOR scheme, without appreciable pulse broadening. Fig. 5 shows the measured SFDR and tunable delay versus Balanced SCISSOR wavelength offset.

These low loss TTD results based on the dual-stripe Si_3N_4 waveguide are impressive, but they lack clear potential to be integrated with active photonic devices such as lasers and modulators. For practical on-chip fully integrated RF beamforming networks, lasers and modulators are required to generate the optical carrier with microwave modulation. High speed

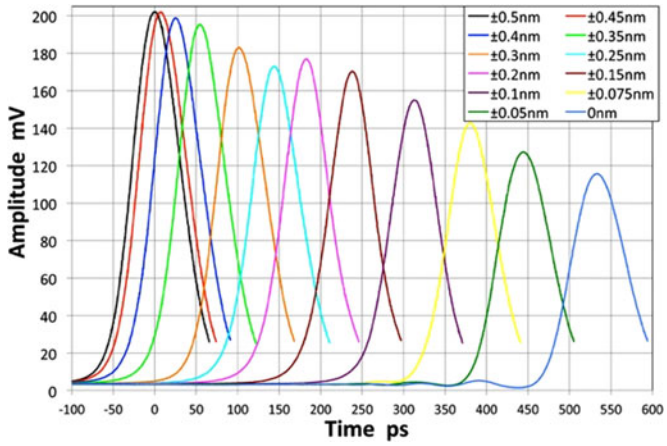

Fig. 4. Delayed optical pulses versus wavelength offset.

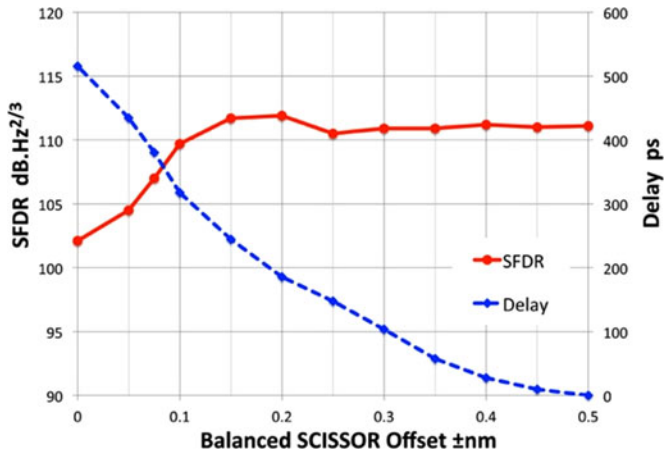

Fig. 5. SFDR and Delay versus wavelength offset.

photodetectors are used to convert the optical signal back into the electrical domain following the RF beamforming function. However, all of these active devices are missing in the monolithic silicon nitride platform. In order to fully benefit from the superior passive properties of silicon nitride, active device integration should also be implemented.

Heterogeneous integration with silicon photonics and III-V materials offers a practical way to implement all of these functions together with silicon nitride based devices [39]. Recent advances show remarkable progress toward integration of Si_3N_4 with Si photonic waveguide [15], [40], III-V/silicon photodetectors [41], etc. A broadband coupling taper between the Si waveguide and ultra-low loss single stripe planar Si_3N_4 waveguide was demonstrated in [42]. It achieved a coupling loss below 0.1 dB between Si and Si_3N_4 waveguides with over 50 nm optical bandwidth. This opens up the possibility to heterogeneously integrate active III-V on silicon devices together with ultra-low loss Si_3N_4 waveguides.

III. Design, Fabrication and Experimental Characterization

Single strip high aspect ratio planar Si_3N_4 waveguides, 40 nm thick, were demonstrated to have waveguide loss as low as

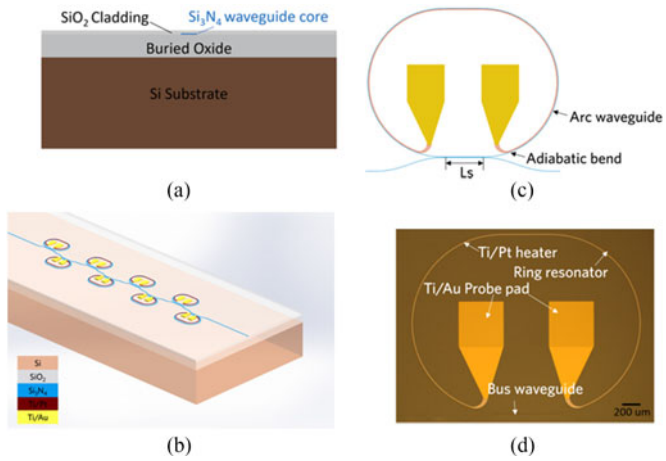

Fig. 6. (a) The waveguide cross section. (b) Schematic illustration of the SCISSOR device with eight racetrack ring resonators. (c), (d) racetrack ring resonator and a corresponding microscope image of the fabricated device.

0.1 dB/m (0.001 dB/cm) in [31], [43], however, such low losses cannot be achieved in ring resonators with practical ring radii for use in TTD devices. The waveguide cross section of devices used in this work is shown in Fig. 6(a). The waveguide core is 2.8 μm wide and 90 nm thick. In order to avoid any substrate leakage, a 15 μm thick thermal oxide layer is grown on the silicon wafer, to be used as the lower cladding. An LPCVD Si_3N_4 layer is then deposited, followed by DUV lithography and ICP dry etch. An SiO_2 layer is deposited after the Si_3N_4 waveguide core formation using PECVD, and then the device is annealed at 1050 °C to remove hydrogen which is detrimental to the waveguide loss. Using electron beam deposition and a liftoff process, Ti/Pt is used as the heater and Ti/Au is used for the electrical probe pads. They together form the thermal tuners to tune the ring resonances.

A schematic view of the device is shown in Fig. 6(b). It has eight racetrack type ring resonators, each with identical dimensions. The ring radius is 1 mm and the straight section is 380 μm long (Ls). To avoid an abrupt connection between the arc ring waveguide and the straight section, an adiabatic bend is used to connect both sections. Meanwhile, the bus waveguide has the same adiabatic section departing the coupling region.

The total circumference of the ring resonator is 7427 μm. Eight rings are placed in pairs on opposite sides of the bus waveguide to avoid thermal crosstalk. They have identical gap width to the bus waveguide in the coupling region. The thermal tuners are placed alongside the ring resonator, avoiding the coupling region. Fig. 6(c) and (d) show a schematic and a photograph of the fabricated ring resonator. The measured group index of the waveguide is $\sim$1.57 and the FSR of the ring is $\sim$25 GHz.

The operation principle of this Balanced SCISSOR tunable TTD is illustrated in Fig. 7, which shows the calculated group delay for the 8-ring device with a coupling constant, κ, of 0.8, while using the Balanced SCISSOR tuning scheme. The rings are separated into two sets and during resonance tuning, one set is blue shifted and one set is red shifted.

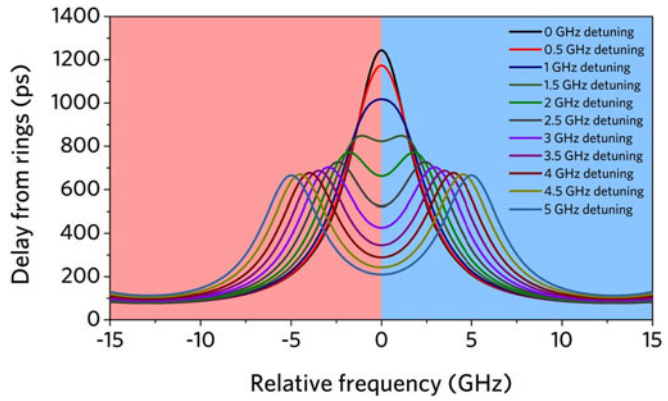

Fig. 7. Calculation of group delay frequency dependence under varied Balanced SCISSOR rings frequency detuning.

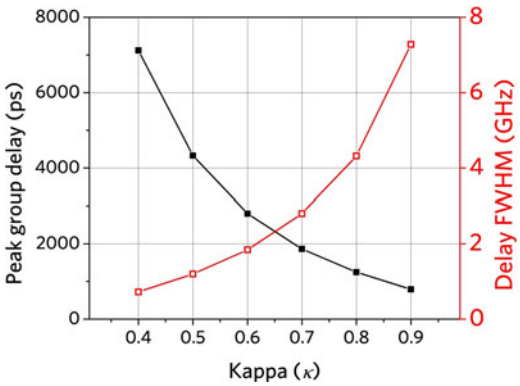

Fig. 8. Calculated dependence of peak group delay and delay FWHM on κ.

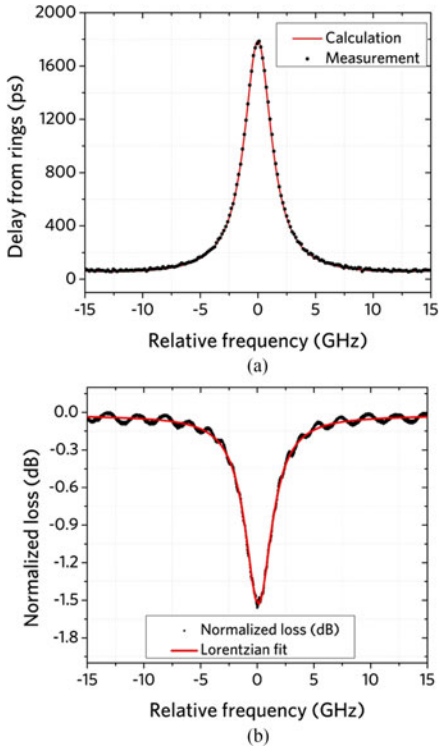

Fig. 9. (a) Measured group delay and (b) normalized loss versus frequency detuning for TTD design with $\kappa = 0.715$ when all the ring resonances are aligned.

In Fig. 7 it can be seen that with no frequency detuning between the two sets of rings, the group delay shows a single peak with a large group delay value, but narrower bandwidth. As the rings are separated in frequency, the group delay at the center frequency is lowered. For higher frequency detuning, the bandwidth of the delay is increased, with a more-flattened delay shape. As detuning increases, the delay continues to decrease until it approaches zero when the detuning value is larger than $\sim$7 GHz.

Once the dimension of ring resonators has been set, the only variable parameter is the ring resonator coupling coefficient κ, chosen by modifying the coupler gap width W. For ring resonators, κ plays an important role in determining the ring spectral shape. For smaller κ values, higher finesse is achieved, giving a narrower bandwidth with longer delay and, therefore, larger loss. As the TTD device consists of cascaded identical ring resonators, the overall response when all the rings are aligned will show the same dependence on the ring coupling coefficient κ. Fig. 8 depicts the calculated dependence of peak delay and delay full width half maximum (FWHM) on κ.

The fabricated devices are characterized using a Luna Optical Vector Analyzer (OVA). A polarization controller, polarizer and polarization maintaining fiber are used to guarantee TE mode operation for all the measurements. The measured group delay frequency dependence for the TTD design with $\kappa = 0.715$, when resonances of all rings are aligned, is shown in Fig. 9(a). For this device, the gap width of the ring couplers is 2.1 μm. A peak delay of 1800 ps with 3 GHz FWHM is achieved. This delay spectrum fits well with the theoretical calculation. The corresponding normalized transmission measurement is plotted in Fig. 9(b). At center frequency, the loss is only 1.6 dB, and the TTD loss spectrum is proportional to the delay spectrum except for small Fabry-Perot ripples due to chip facet reflections. From this resonance dip and peak delay value, a low loss of $\sim$0.89 dB/ns is calculated, a record loss/delay value. As the group index is 1.57, this corresponds to 4.65 dB/m for all loss contributions including the propagation loss, radiation loss and excess coupler loss. This low loss value benefits from the ultra-low loss Si_3N_4 waveguide as well as the careful designs of adiabatic connections and ring couplers.

When all the ring resonances are aligned, although the peak delay is large, it rolls off quickly giving a narrow bandwidth. As discussed in the previous section, this is mitigated by applying frequency detuning. Using Balanced SCISSOR operation, the delay is flattened around the center frequency with 1 GHz detuning, as shown in Fig. 10. At the same time, the loss also becomes flattened at the resonance dip. A loss of $\sim$1 dB together with a flattened top with 1.2 ns group delay are achieved. The FWHM is measured to be 5 GHz, in close agreement with calculations. This flattened spectrum will result in far less distortion for RF signals with a large bandwidth.

The calculated and measured group delay for Balanced SCISSOR operation at various frequency detunings, for the device with $\kappa = 0.715$, are shown in the Fig. 11. Continuously

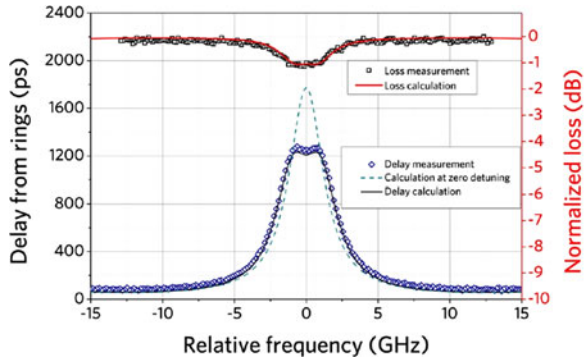

Fig. 10. Measured group delay and normalized loss versus frequency detuning for SCISSOR design with $\kappa = 0.715$, at 1 GHz frequency detuning.

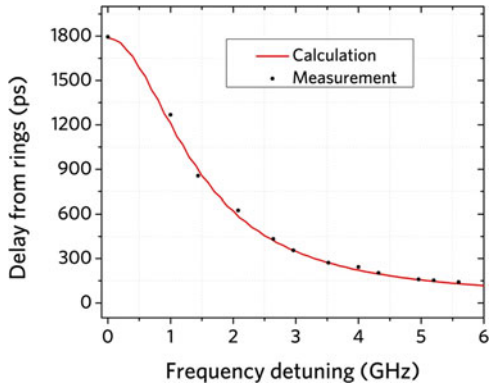

Fig. 11. Tunable delay operation on SCISSOR $\kappa = 0.715$; summarized group delay versus frequency detuning dependence.

tunable delay of 1800 ps is demonstrated by varying the frequency detuning from 0 to over 6 GHz.

As the Balanced SCISSOR resonance gets tuned "in" and "out," not only the delay value but also the FWHM changes, and this fact provides some flexibility in device operation. Once a TTD design is fixed, both the maximum achievable delay and the FWHM can be tailored to some extent to support different applications.

It is worthy to mention that, for this type of SCISSOR device, the kappa value could be made tunable by using an MZI at the coupling region of the ring resonator and bus waveguide. This would offer additional tunability of the delay range and bandwidth, however, it would come with a higher coupler loss.

Once ring resonance alignment is achieved from initial tuning, the rings are separated into two groups with different thermal tuning direction, keeping the overall heating almost constant [29]; this eliminates the overall changing in power dissipation from delay tuning, and results in a faster tuning speed due to the elimination of any long-time transient. It should be mentioned that, due to its low thermo-optic coefficient, Si_3N_4 is quite insensitive to thermal tuning. This insensitivity also helps to achieve more stable and finer tuning of the rings in order to achieve a more accurate resonance detuning and delay spectra flattening. However, in order to improve the thermal tuning efficiency, a viable option is to undercut the silicon substrate, to reduce the heat dissipation and concentrate heat around the waveguide core.

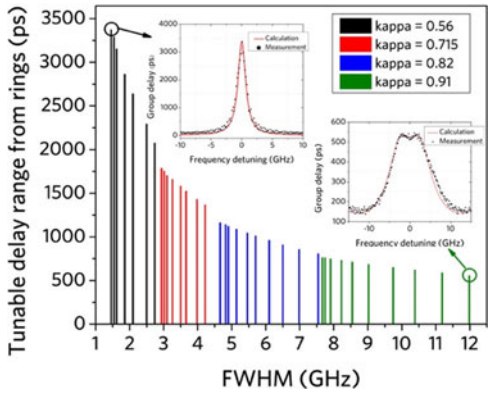

Fig. 12. A summary of the tunable delay range and FWHM for different κ.

For devices with different κ values, the design can give a range of achievable delay/FWHM combinations. Fig. 12 summarizes four designs where only the delay range change between the peak delay and flat top response are listed. A maximum delay of 3.4 ns is achieved with a design having a κ of 0.56 when all the rings are aligned in resonance as shown in the inset. For a design with a higher κ of 0.91, at a frequency detuning of 2.5 GHz, the FWHM was extended to 12 GHz, with flat top response of ~520 ps group delay across a wide band, with fluctuations within ~15 ps. It is worthwhile to mention that the delay bandwidth can also be increased by setting the frequency detuning large enough where the two set of peaks are separated further to utilize the tail of the frequency response. This can be seen by the curve in Fig. 7, which has a 5 GHz frequency detuning and very flat group delay around the center frequency.

In order to compare the performance of our SCISSOR device with recent demonstrated state-of-the-art TTD devices, we summarized several key aspects of TTD performance including Delay Range, Tuning Resolution, Working Bandwidth, Delay Loss, Power Efficiency, and Device Footprint in Table I. [30] gives an overview of various approaches and here we mainly summarize TTD devices which could provide hundreds of ps delay, as required for a practical RF beamforming system. While different approaches provide different advantages, our device results provide superior low loss; 0.89 dB loss per ns delay. This can be compared with 60 dB loss per ns of delay for the silicon counterparts using the same balanced SCISSOR operation principle, however, at the expense of a significantly larger device footprint. Additionally, the use of a single stripe Si3N4 waveguide provides the potential for full heterogeneous integration with III-V/Si active devices.

IV. Discussion

A. Excess Coupler Loss

Reduction of the total insertion loss of the device is a key motivator to use ultra-low loss Si_3N_4 waveguides instead of silicon waveguides for the TTD devices. The low propagation loss of Si_3N_4 waveguides largely reduces the signal loss from multiple round trips of propagation within the ring resonator. Careful design of the adiabatic transition between the straight

TABLE I
A SUMMARY OF STATE-OF-THE-ART TTD DEVICES

	Delay range (ps)	Resolution (ps)	Bandwidth (GHz)	Delay loss (dB/ps)	Power efficiency (mW/ps)	Footprint (mm^2)
Si SCISSOR	345	Small	10	0.06	0.07	0.125
Si_3N_4/SiO_2 MZI and ring resonator	~12000	Small	——	~1.8E-3	——	——
Si MZI and ring resonator	1280	Small	60	0.01	0.05	28.62
Si_3N_4 MZI and waveguide spiral	12350	850	Large	1.9E-4	0.02	3825
*Our Work (Si_3N_4 SCISSOR)**	1800	Small	3	8.9E-4	0.13	90

*Device with kappa of 0.715 when all the rings are aligned in resonance. The delay range and bandwidth might vary across designs and under balanced SCISSOR operation. Some of the parameters for comparison works are taken from [30].

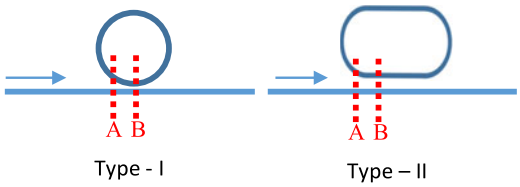

Fig. 13. Illustration and comparison of two types (type-I normal curve-straight and type-II racetrack) of ring couplers.

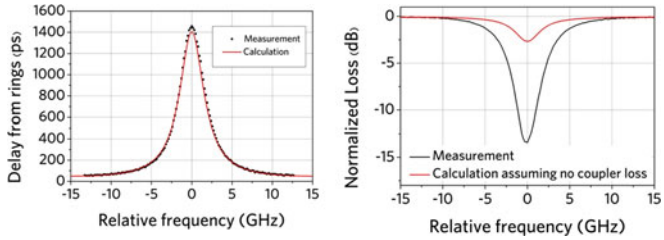

Fig. 14. Delay and loss versus frequency from prior design with large loss.

and the bending arc waveguide reduces the radiation loss due to curvature mismatch. However, in addition to the loss within the ring resonator itself, the ring coupler to the bus waveguide adds excess loss. This loss is investigated thoroughly in [44], and specifically for a ring resonator with a large κ value, this loss can become a large contributor to the total loss. The excess loss originates from the mode conversion at the coupling region and will increase as the mode mismatch increases when light approaches the coupling region from the bus waveguide. Normally, this mode mismatch depends on the gap width between the bus waveguide and the ring resonator. For a smaller gap, more super eigen-mode difference can be seen between the cross-section A and B depicted in Fig. 13. As the transition might not be perfectly adiabatic within such a small distance, this can result in a large mode conversion loss. However, by increasing the gap width, the mode mismatch will be reduced and this mode transition will more likely become an adiabatic process, resulting a much lower excess loss.

The mode conversion loss is usually neglected in cases where the propagation loss is relatively high, without too much contribution from excess coupler loss. However, for ultra-low loss waveguides and ring resonators, this coupler loss should be considered as it can become comparable to or even higher than the single trip propagation loss within the ring resonator. Spencer *et al.* provide details of different coupler designs to achieve low loss ring couplers for the use in integrated ultra-high Q factor ring resonators [45]. In summary, a weakly tapered pulley coupler enables a more adiabatic transition at the coupling region, giving very low excess coupler loss. However, for the TTD designs, the ring resonators operate in the over-coupled regime and a large value of κ is required. Due to the weak mode confinement, pulley couplers which use concentric curved waveguides at the coupling region include a mode asymmetry between the bus waveguide and the ring waveguide. This limits the maximum achievable κ and makes the pulley coupler less suited to the TTD designs. The mode asymmetry in pulley couplers could be reduced by using asymmetric waveguide structures, but this adds significant complexity to the waveguide design.

Compared with a normal curve-straight type-I ring coupler, the type-II racetrack ring couplers adopted in this work provide a much longer coupling length. This inherently allows for a larger coupling gap width to achieve the same coupling ratio, κ. Fig. 14 shows the measurement results of a TTD device from a prior run, which used type-I ring couplers. It has 3.66 GHz FWHM and a nicely matched group delay spectrum with the calculation. However, the total loss is as high as 10 dB while an independent loss measurement shows only ~8 dB/m waveguide loss. Considering a lossless coupler, 8 dB/m propagation loss should give only ~2.5 dB total loss. This unexpected high loss originated from the small gap width (560 nm) used for this device, which induces too much coupler loss. In racetrack type designs, a similar κ value can be achieved with a gap width around 2.1 μm, which greatly reduces the excess coupler loss as well as the total loss of the device.

B. Flexible Use of the Rings

For this type of TTD design, longer delay can be achieved by increasing the number of rings. It can be seen that, with N ring resonators, it is also possible to use the device as an M-ring TTD device (M < N), by shifting (N-M) ring resonances well away from the signal frequency. This helps to screen out some ring resonators which might show unexpected higher loss from fabrication imperfections, such as defects in the SiO_2 upper cladding layer around the ring waveguide.

C. Group Delay Dispersion

Group delay dispersion (GDD) $\partial T/\partial\omega$ was also measured for different TTD designs and operation conditions using the LUNA OVA unit. As introduced in previous sections, the Balanced SCISSOR operation significantly cancels the third order

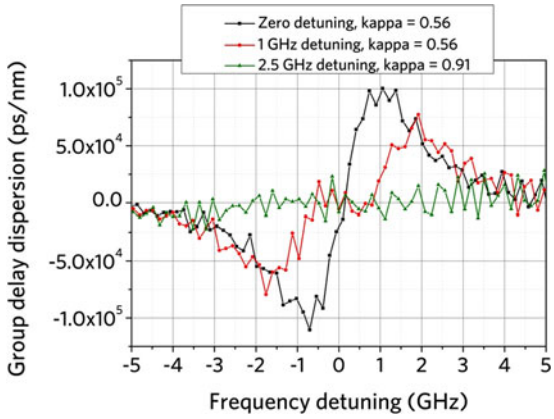

Fig. 15. Group delay dispersion measurement for three SCISSOR designs and operations. Black: $\kappa = 0.56$, zero detuning; red: $\kappa = 0.56$, 1 GHz detuning; green: $\kappa = 0.91$, 2.5 GHz detuning.

dispersion around the center frequency and thus increases the operation bandwidth. The measured GDD is shown in Fig. 15 for a TTD design with a κ of 0.56. At the central frequency, the GGD is always zero due to symmetry of the Balanced Scissor, but away from that central frequency the GDD increases as $\partial T/\partial\omega \sim \partial^2 T/\partial\omega^2 \times (\omega - \omega_0) + \ldots$ Since, as mentioned in Section II the second order GDD $\partial^2 T/\partial\omega^2$ is reduced in the Balanced SCISSOR as the rings are detuned, the maximum GDD is decreased with resonator detuning. This leads to a flattened delay compared with the case with zero resonator detuning, which was discussed for Figs. 9 and 10. For an even larger κ value of 0.91 with larger resonator detuning of 2.5 GHz, the GDD keeps at a low value around the center frequency across over 9 GHz range. This results in a wideband group delay spectrum, as shown in the inset of Fig. 12. These measurements validate the theoretical analysis of third and higher order dispersion influence on the group delay bandwidth in previous sections. This indicates further chromatic dispersion engineering methods could help extend the operating bandwidth of these TTD devices.

V. Summary and Conclusion

In summary, continuously tunable true time delay (TTD) devices based on Si_3N_4 ring resonators are demonstrated. The loss associated with the delay is as low as 0.89 dB/ns, due to the ultralow propagation loss of high aspect ratio Si_3N_4 waveguides and careful design of the ring coupler to minimize excess coupler loss. Balanced SCISSOR operation is used to achieve a tunable delay from 0 to 3.4 ns. The device bandwidth and peak delay range can be flexibly designed by modifying the ring coupler design, and to some extent the resonance frequency detuning, suitable for different application requirements. A device with over 10 GHz bandwidth and a flattened delay of over 500 ps is demonstrated, enabling distortion free TTD operation of microwave signals. As this device design has the potential to be integrated with active devices through heterogeneous integration on the silicon photonics platform, it holds great promise for being used for photonic integrated circuits in practical microwave photonics applications.

References

[1] Y. Vlasov, "Silicon CMOS-integrated nano-photonics for computer and data communications beyond 100G," *IEEE Commun. Mag.*, vol. 50, no. 2, pp. s67–s72, Feb. 2012.
[2] L. A. Coldren *et al.*, "High performance InP-Based photonic ICs—A tutorial," *J. Light. Technol.*, vol. 29, no. 4, pp. 554–570, Feb. 2011.
[3] G. Roelkens *et al.*, "III-V/silicon photonics for on-chip and intra-chip optical interconnects," *Laser Photon. Rev.*, vol. 4, no. 6, pp. 751–779, Nov. 2010.
[4] Y. Chen, H. Lin, J. Hu, and M. Li, "Heterogeneously integrated silicon photonics for the mid-infrared and spectroscopic sensing," *ACS Nano*, vol. 8, no. 7, pp. 6955–6961, Jul. 2014.
[5] M. J. R. Heck *et al.*, "Hybrid silicon photonic integrated circuit technology," *IEEE J. Sel. Topics Quantum Electron.*, vol. 19, no. 4, Jul. 2013, Art. no. 6100117.
[6] J. Yao, "Microwave photonics," *J. Light. Technol.*, vol. 27, no. 3, pp. 314–335, Feb. 2009.
[7] P. A. Morton and Z. Mizrahi, "Low-cost, low-noise hybrid lasers for high SFDR RF photonic links," in *Proc. 2012 IEEE Avionics, Fiber Opt. Photon. Technol. Conf.*, 2012, pp. 64–65.
[8] P. A. Morton, M. Morton, and S. Morton, "Ultra low phase noise, high power, hybrid lasers for RF mixing and optical sensing applications," in *Proc. IEEE Avionics Veh. Fiber Opt. Photon. Technol. Conf.*, 2017, Paper TuB.1.
[9] A. W. Fang *et al.*, "Electrically pumped hybrid AlGaInAs-silicon evanescent laser," *Opt. Exp.*, vol. 14, no. 20, pp. 9203–9210, Oct. 2006.
[10] A. Y. Liu *et al.*, "High performance continuous wave 1.3 μm quantum dot lasers on silicon," *Appl. Phys. Lett.*, vol. 104, no. 4, Jan. 2014, Art. no. 41104.
[11] D. Huang *et al.*, "Dynamically reconfigurable integrated optical circulators," *Optica*, vol. 4, no. 1, pp. 23–30, Jan. 2017.
[12] P. Pintus *et al.*, "Integrated widely tunable broadband optical isolator," in *Proc. 43rd Eur. Conf. Opt. Commun.*, 2017, Paper W.1.C.3.
[13] C. Zhang, P. A. Morton, J. B. Khurgin, J. D. Peters, and J. E. Bowers, "Highly linear heterogeneous-integrated Mach-Zehnder interferometer modulators on Si," *Opt. Exp.*, vol. 24, no. 17, pp. 19040–19047, Aug. 2016.
[14] C. Zhang, P. A. Morton, J. B. Khurgin, J. D. Peters, and J. E. Bowers, "Ultralinear heterogeneously integrated ring-assisted Mach–Zehnder interferometer modulator on silicon," *Optica*, vol. 3, no. 12, pp. 1483–1488, Dec. 2016.
[15] M. J. R. Heck, J. F. Bauters, M. L. Davenport, D. T. Spencer, and J. E. Bowers, "Ultra-low loss waveguide platform and its integration with silicon photonics," *Laser Photon. Rev.*, vol. 8, no. 5, pp. 667–686, Sep. 2014.
[16] E. Rouvalis *et al.*, "High-Power and high-linearity photodetector modules for microwave photonic applications," *J. Light. Technol.*, vol. 32, no. 20, pp. 3810–3816, Oct. 2014.
[17] Z. Li *et al.*, "High-power high-linearity flip-chip bonded modified unitraveling carrier photodiode," *Opt. Exp.*, vol. 19, no. 26, pp. B385–B3890, Dec. 2011.
[18] M. Y. Frankel and R. D. Esman, "True time-delay fiber-optic control of an ultrawideband array transmitter/receiver with multibeam capability," *IEEE Trans. Microw. Theory Tech.*, vol. 43, no. 9, pp. 2387–2394, Sep. 1995.
[19] I. Frigyes and A. J. Seeds, "Optically generated true-time delay in phased-array antennas," *IEEE Trans. Microw. Theory Tech.*, vol. 43, no. 9, pp. 2378–2386, Sep. 1995.
[20] Z. Cao *et al.*, "Advanced integration techniques on broadband millimeter-wave beam steering for 5G wireless networks and beyond," *IEEE J. Quantum Electron.*, vol. 52, no. 1, Jan. 2016, Art. no. 0600620.
[21] M. Longbrake, "True time-delay beamsteering for radar," in *Proc. 2012 IEEE Nat. Aeros. Electron. Conf.*, 2012, pp. 246–249.
[22] D. Marpaung *et al.*, "Integrated microwave photonics," *Laser Photon. Rev.*, vol. 7, no. 4, pp. 506–538, Jul. 2013.
[23] J. B. Khurgin, "Expanding the bandwidth of slow-light photonic devices based on coupled resonators," *Opt. Lett.*, vol. 30, no. 5, pp. 513–515, Mar. 2005.
[24] J. B. Khurgin and P. A. Morton, "Tunable wideband optical delay line based on balanced coupled resonator structures," *Opt. Lett.*, vol. 34, no. 17, pp. 2655–2657, Sep. 2009.
[25] J. Cardenas *et al.*, "Wide-bandwidth continuously tunable optical delay line using silicon microring resonators," *Opt. Exp.*, vol. 18, no. 25, pp. 26525–26534, Dec. 2010.

[26] J. K. S. Poon, J. Scheuer, Y. Xu, and A. Yariv, "Designing coupled-resonator optical waveguide delay lines," *J. Opt. Soc. Amer. B*, vol. 21, no. 9, pp. 1665–1673, Sep. 2004.
[27] A. Melloni *et al.*, "Tunable delay lines in silicon photonics: coupled resonators and photonic crystals, a comparison," *IEEE Photon. J.*, vol. 2, no. 2, pp. 181–194, Apr. 2010.
[28] P. A. Morton and J. B. Khurgin, "Microwave photonic delay line with separate tuning of the optical carrier," *IEEE Photon. Technol. Lett.*, vol. 21, no. 22, pp. 1686–1688, Nov. 2009.
[29] P. A. Morton, J. Cardenas, J. B. Khurgin, and M. Lipson, "Fast thermal switching of wideband optical delay line with no long-term transient," *IEEE Photon. Technol. Lett.*, vol. 24, no. 6, pp. 512–514, Mar. 2012.
[30] X. Wang *et al.*, "Continuously tunable ultra-thin silicon waveguide optical delay line," *Optica*, vol. 4, no. 5, pp. 507–515, May 2017.
[31] J. F. Bauters *et al.*, "Planar waveguides with less than 01 dB/m propagation loss fabricated with wafer bonding," *Opt. Exp.*, vol. 19, no. 24, pp. 24090–24101, Nov. 2011.
[32] D. Dai, J. Bauters, and J. E. Bowers, "Passive technologies for future large-scale photonic integrated circuits on silicon: Polarization handling, light non-reciprocity and loss reduction," *Light Sci. Appl.*, vol. 1, 2012.
[33] M. Burla *et al.*, "On-chip CMOS compatible reconfigurable optical delay line with separate carrier tuning for microwave photonic signal processing," *Opt. Exp.*, vol. 19, no. 22, pp. 21475–21484, Oct. 2011.
[34] L. Zhuang *et al.*, "Low-loss, high-index-contrast Si_3N_4/SiO_2 optical waveguides for optical delay lines in microwave photonics signal processing," *Opt. Exp.*, vol. 19, no. 23, pp. 23162–23170, Nov. 2011.
[35] C. G. H. Roeloffzen *et al.*, "Silicon nitride microwave photonic circuits," *Opt. Exp.*, vol. 21, no. 19, pp. 22937–22961, Sep. 2013.
[36] P. A. Morton, J. Khurgin, Z. Mizrahi, and S. Morton, "Commercially packaged optical true-time-delay devices with record delays of wide bandwidth signals," in *Proc. Conf. Lasers Electro-Opt.*, 2014, Paper AW3P.6.
[37] J. Cardenas, P. A. Morton, J. B. Khurgin, C. B. Poitras, and M. Lipson, "Super-Ring resonators: Taking advantage of resonance variability," in *Proc. 2012 Conf. Lasers Electro Opt.*, 2012, Paper CTu3I.4.
[38] P. A. Morton, J. B. Khurgin, Z. Mizrahi, and S. J. Morton, "High SFDR 'Super-Ring' microresonator based True-Time-Delay (TTD)," in *Proc. 2014 IEEE Avionics, Fiber Opt. Photon. Technol. Conf.*, 2014, pp. 27–28.
[39] T. Komljenovic *et al.*, "Heterogeneous silicon photonic integrated circuits," *IEEE J. Lightw. Technol.*, vol. 34, no. 1, pp. 20–35, Jan. 1, 2016.
[40] J. F. Bauters *et al.*, "Silicon on ultra-low-loss waveguide photonic integration platform," *Opt. Exp.*, vol. 21, no. 1, pp. 544–555, Jan. 2013.
[41] J. F. Bauters, J. E. Bowers, M. J. R. Heck, M. L. Davenport, and M. Piels, "Low-loss Silicon Nitride AWG demultiplexer heterogeneously integrated with hybrid III–V/Silicon Photodetectors," *J. Light. Technol.*, vol. 32, no. 4, pp. 817–823, Feb. 2014.
[42] M. L. Davenport and J. E. Bowers, "Efficient and broad band coupling between silicon and ultra-low-loss silicon nitride waveguides," in *Proc. 2016 IEEE Photon. Conf.*, 2016, pp. 631–632.
[43] J. F. Bauters *et al.*, "Ultra-low-loss high-aspect-ratio Si_3N_4 waveguides," *Opt. Exp.*, vol. 19, no. 4, pp. 3163–3174, Feb. 2011.
[44] F. Xia, L. Sekaric, and Y. A. Vlasov, "Mode conversion losses in silicon-on-insulator photonic wire based racetrack resonators," *Opt. Exp.*, vol. 14, no. 9, pp. 3872–3886, May 2006.
[45] D. T. Spencer, J. F. Bauters, M. J. R. Heck, and J. E. Bowers, "Integrated waveguide coupled Si_3N_4 resonators in the ultrahigh-Q regime," *Optica*, vol. 1, no. 3, pp. 153–157, Sep. 2014.

Chao Xiang (S'xx) received the B.E. degree in optoelectronic information engineering from Huazhong University of Science and Technology, Wuhan, China, in 2012 and the M.Phil. degree in information engineering from Chinese University of Hong Kong, Hong Kong, in 2014. He is currently working toward the Ph.D. degree in the Department of Electrical and Computer Engineering, University of California, Santa Barbara, CA, USA. His current research interests include applications of silicon photonics.

Michael L. Davenport received the undergraduate degree in optical engineering from the University of Alabama, Huntsville, AL, USA, in 2007, and the Ph.D. degree in electrical engineering from the University of California, Santa Barbara, CA, USA, in 2017. His research interests include low-noise mode-locked lasers for applications in optical networks.

Jacob B. Khurgin (SM'xx) received the M.S. degree in optics from the Institute of Fine Mechanics and Optics, St. Petersburg, Russia, in 1979 and the Ph.D. degree in electro-physics Polytechnic Institute of New York, Brooklyn, NY, USA, in 1987. In 1980, he emigrated to the U.S. and had joined Philips Laboratories, NV Philips, Briarcliff Manor, NY, USA, where he worked for eight years and was engaged in research on miniature solid-state lasers, II–VI semiconductor lasers, various display and lighting fixtures, X-ray imaging, and small appliances. In January 1988, he joined the Department of Electrical and Computer Engineering, Johns Hopkins University, Baltimore, MD, USA, where he is currently a Professor. He is the author or coauthor of more than 300 papers published in refereed journals, five book chapters, one book edited. He is the holder of 34 patents. His research interests include eclectic mixture of optics of semiconductor nanostructures, nonlinear optical devices, optical communications, microwave photonics, Terahertz Technology, condensed matter physics, mid-infrared lasers, plasmonics, laser cooling, RF photonics, IR detectors, phonon engineering for high-frequency transistors, coherent optical communications, and slow light propagation. He is a Fellow of the Optical Society of America.

Paul A. Morton (F'11) received the B.Sc., M.Eng., and Ph.D. degrees in electrical engineering from the University of Bath, Bath, U.K. He was a Postdoctoral Researcher with the University of California, Santa Barbara, CA, USA, before becoming a member of technical staff at AT&T Bell Laboratories, Murray Hill, where he made fundamental research contributions in the areas of high-speed laser diodes, mode-locked optical pulse sources, and photonic integration. At CIENA Corporation, he was a Technical Leader in the development of commercial high capacity DWDM transmission and switching systems. He co-founded Morton Photonics, which develops photonic components, photonic integrated circuits utilizing heterogeneous integration, and subsystems based on these devices, for applications of high performance analog RF Photonic links, sensing, and photonic processing for phased array sensors. He has authored or coauthored two book chapters, more than 100 journal and conference papers, and holds 11 patents. He is a Fellow of the Optical Society of America.

John E. Bowers (F'93) received the M.S. and Ph.D. degrees from Stanford University, Stanford, CA, USA. He is a Professor with the Department of Electrical and Computer Engineering, University of California, Santa Barbara, CA, USA, where he is the Fred Kavli Chair in Nanotechnology and the Director of the Institute for Energy Efficiency. He was also with AT&T Bell Laboratories and Honeywell. He has authored or coauthored eight book chapters, 450 journal papers, and 700 conference papers. He holds 52 patents. He is a member of the National Academy of Engineering, and a Fellow of the Optical Society of America (OSA), and the American Physical Society. He received the OSA/IEEE Tyndall Award, the OSA Holonyak Prize, the IEEE LEOS William Streifer Award, the IEEE Photonics Award and the South Coast Business and Technology Entrepreneur of the Year Award. He received the EE Times Annual Creativity in Electronics Award for Most Promising Technology for the hybrid silicon laser in 2007.